ACS OMEGA

http://pubs.acs.org/journal/acsodf

Article

Effects of Distal Mutations on Ligand-Binding Affinity in *E. coli* Dihydrofolate Reductase

Chen-Hua Huang,[‖] Yun-Wen Chen,[‖] Tsun-Tsao Huang, and Ya-Ting Kao*

Cite This: *ACS Omega* 2021, 6, 26065−26076

Read Online

ACCESS | Metrics & More | Article Recommendations | Supporting Information

ABSTRACT: Mutations far from the center of chemical activity in dihydrofolate reductase (DHFR) can affect several steps in the catalytic cycle. Mutations at highly conserved positions and the distal distance of the catalytic center (Met-42, Thr-113, and Gly-121) were designed, including single-point and double-point mutations. Upon ligand binding, the fluorescence of the intrinsic optical probe, tryptophan, decreases due to either fluorescence quenching or energy transfer. We demonstrated an optical approach in measuring the equilibrium dissociation constant for enzyme−cofactor, enzyme−substrate, and enzyme−product complexes in wildtype *ec*DHFR and each mutant. We propose that the effects of these distal mutations on ligand-binding affinity stem from the spatial steric hindrance, the disturbance on the hydrogen network, or the modification of the protein flexibility. The modified N-terminus tag in DHFR acts as a cap on the entrance of the substrate-binding cavity, squeezes the adenosine binding subdomain, and influences the binding of NADPH in some mutants. If the mutation positions are away from the N-terminus tag and the adenosine binding subdomain, the additive effects due to the N-terminus tag were not observed. In the double-mutant-cycle analysis, double mutations show nonadditive properties upon either cofactor or substrate binding. Also, in general, the first point mutation strongly affects the ligand binding compared to the second one.

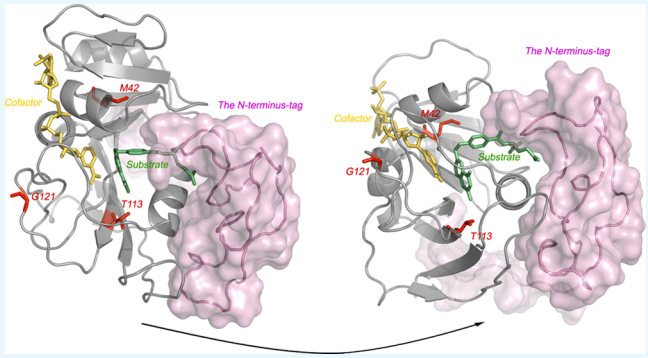

INTRODUCTION

The enzyme dihydrofolate reductase (DHFR) catalyzes the reduction of 7,8-dihydrofolate (H_2F) to 5,6,7,8-tetrahydrofolic acid (H_4F) with nicotinamide adenine dinucleotide phosphate (NADPH) as the cofactor. The catalytic product H_4F is essential for amino acid catabolism. Hence, DHFR has been recognized as a target for anticancer drugs and antibacterial agents, such as methotrexate (MTX) and trimethoprim (TMP).[1,2] *Escherichia coli* DHFR (*ec*DHFR) is a monomeric protein of 159 amino acid residues (∼18 kD). There are over 40 structures of *ec*DHFR in both binary and ternary complexes states.[3−5] Its three-dimensional structure is dominated by a central eight-stranded β-sheet (strands βA−βH) with four α-helices (αB, αC, αE, and αF) flanking around. The enzyme comprises the adenosine binding subdomain (residues 38−88) and the major subdomain, also named loop subdomain, encompassing the binding sites for the cofactor and the substrate. The loop subdomain contains three critical loops: the Met20 loop (residues 9−24) closes over the active-site pocket, and the βF−βG (residues 116−132) and βG−βH (residues 142−150) loops stabilize the various conformations of the Met20 loop. The substrate and the cofactor bind in a deep hydrophobic cleft at the juncture of the two subdomains. The nicotinamide ring of NADPH is coplanar with the β-sheet and spans the gap between strands βA and βE. The pteridine ring of H_2F fits into the cleft between helices αB and αC.

Previous studies have shown that the mutations far from the center of chemical activity in DHFR can affect several steps in the catalytic cycle.[6−13] Among these studies, the distal residues Gly-121 and Met-42 are highly conserved. The double-mutant enzymes in which Gly-121 and Met-42 are both substituted exhibit synergistic reduction in the hydride transfer rate.[7−10] Gly-121 is located on the βF−βG loop and next to Asp-122, forming hydrogen bonds with Glu-17 and Gly-15 on the Met20 loop. A mutation on this neighboring residue Gly-121 leads to a decrease in the rate of hydride transfer.[6] Met-42 is located on the strand βB and close to the Trp-47 on helix αC. The helix αC is in the adenosine binding subdomain and directly interacts with the Met20 loop associating to the cofactor binding and catalytic reaction. Also, Asp-27 is near the active site and plays an essential role in facilitating the proton

Received: June 8, 2021
Accepted: September 22, 2021
Published: October 1, 2021

transfer and hydride transfer steps. Asp-27 may help to orient the substrates and the water molecule through various electrostatic interactions.[14−17] Another conserved residue Thr-113 is located in strand βF, away from the adenosine binding subdomain but forming hydrogen bonding with Asp-27.[5,14]

We systematically measured the equilibrium thermodynamic dissociation constant for enzyme−cofactor, enzyme−substrate, and enzyme−product complexes in wildtype ecDHFR and each mutant. We selected residues at highly conserved positions but different domains (Met-42, Thr-113, and Gly-121) to carry out single and double mutation. We further analyzed the free energy changes to determine the mutation effect on the ligand affinity and possibly on the reaction activity.

RESULTS AND DISCUSSION

Enzyme Activity Assays. The *E. coli* DHRF sequence with a 19-residue lysine biotinylation signal sequence inserted at the N terminal (MGLNDIFEAQKIEWHGGGT; bioseq)[18] was subcloned into the pET28a plasmid. The pET28a-6Histag-bioseq-*ec*DHFR construct was used to express *ec*DHFR, according to the previous report with some modifications.[18] Three mutation points (Met-42, Thr-113, and Gly-121) are highly conserved and distal to the catalytic center, as shown in Figure 1A. We designed these mutations with possible minor disturbance in an active-site structure but with more effects in the local conformation and the interaction network. The residue Met-42 is on the strand βB and in the proximity of helix αC. It was proposed that Met-42 and the helix αC exhibit the correlated motion in wildtype.[9] In previous studies, the forward hydride transfer rates decreased 1.4 times in M42F and displayed negligible changes in M42A and other mutations involving smaller amino acids.[8] Moreover, with a more massive replacement, M42W, the forward hydride transfer rate decreased 41 times. Hence, we replaced Met residue with the bulky Phe residue (M42F) to induce hindrance in the correlated motion. The Gly-121 is located at the center of the βF−βG loop and is 19 Å from the catalytic center. The βF−βG loop is quite flexible and adopts several conformations during catalytic processes.[4] In previous studies, the forward hydride transfer rates decreased 163 and 62 times in G121V and G121S, respectively.[8] Val residue and Ser residue are similar in dimension but have different polarities. We replaced Gly residue with either Val or Ser residues to induce a disturbance in loop motion. Thr-113 is located in βF and forms hydrogen bonding with Asp-27. In previous studies, the forward hydride transfer rates decreased 1.3 times in T113V.[19] Thr residue and Val residue are similar in dimension but have different polarities. We replaced Thr residue with Val to induce a disturbance in the hydrogen network at the catalytic center. Site-directed mutagenesis steps were carried out to engineer the following mutations: (1) single-point mutation: M42F-*ec*DHFR, T113V-*ec*DHFR, G121S-*ec*DHFR, and G121V-*ec*DHFR, (2) double-point mutation: M42F/G121S-*ec*DHFR, M42F/G121V-*ec*DHFR, T113V/G121S-*ec*DHFR, and T113V/G121V-*ec*DHFR. Some mutations have been studied previously and are used for comparison. Some of the mutations are investigated for the first time here.

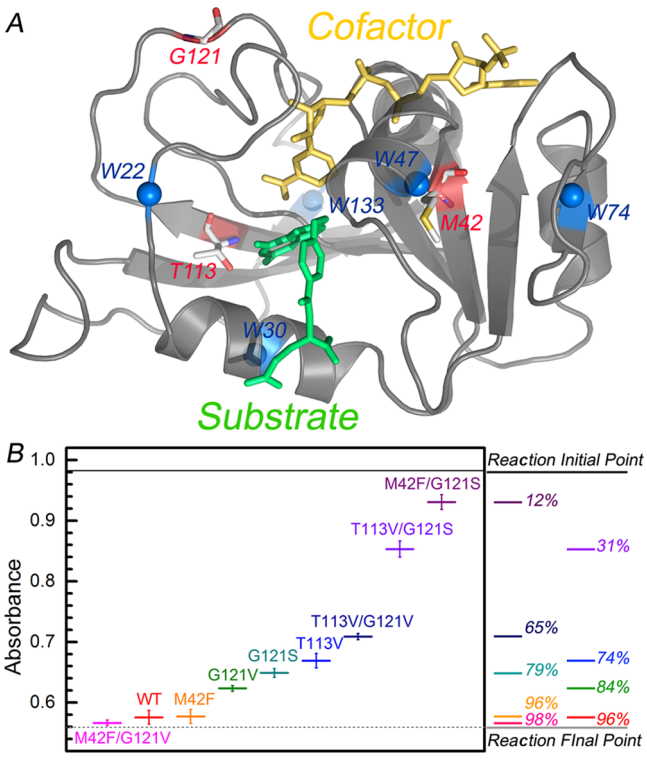

Figure 1. (A) Crystal structure of *ec*DHFR (PDB: 1RX2). Five blue spheres represent the tryptophan amino acid residues (W22/W30/W47/W74/W133). The yellow and green sticks represent the cofactor and substrate. The red labels are the mutation sites (M42, T113V, and G121). (B) Results of enzyme activity assays in wildtype and each mutant. The percentage of the H_2F−to−H_4F conversion was estimated by eq 1.

The activity of *ec*DHFR was determined at 25 °C following the decrease of NADPH and H_2F by the absorbance measurements at 340 nm. The reaction MTEN buffer[20] at pH 7.4 containing the reaction solutions (5 μM *ec*DHFR, 100 μM NADPH, and 50 μM H_2F) were kept at 25 °C, while the absorption measurements were performed for 15 min, and the 15 min endpoint absorbance was recorded. Because *ec*DHFR and $NADP^+$ exhibit no absorption at 340 nm, we estimated the initial point of reaction with a mixture of 100 μM NADPH and 50 μM H_2F and the final point of reaction with a mixture of 50 μM NADPH and 50 μM H_4F. The concentrations of compounds in solution were determined by UV absorbance using the molar extinction coefficients from the previous study.[21]

The 340 nm absorbances of the initial point and the final point are 0.98 and 0.56, respectively. The percentage of the H_2F−to−H_4F conversion in each mutant was estimated by

$$\text{conversion } \% = \frac{(A_{\text{inital point}} - A_{\text{15-minute endpoint}})}{(A_{\text{inital point}} - A_{\text{final point}})} \times 100\% = \frac{(0.98 - A_{\text{15-minute endpoint}})}{(0.98 - 0.56)} \times 100\% \quad (1)$$

All the mutants show catalytic activity with different levels of the substrate-to-product conversion. M42F-*ec*DHFR and M42F/G121V-*ec*DHFR show a similar conversion level as the wildtype, while others show lower conversion levels, especially M42F/G121S-*ec*DHFR and T113V/G121S-*ec*DHFR. Because the initial 5 μM concentration of *ec*DHFR is high, we observed the endpoint results occurring right after

https://doi.org/10.1021/acsomega.1c02995
ACS Omega 2021, 6, 26065−26076

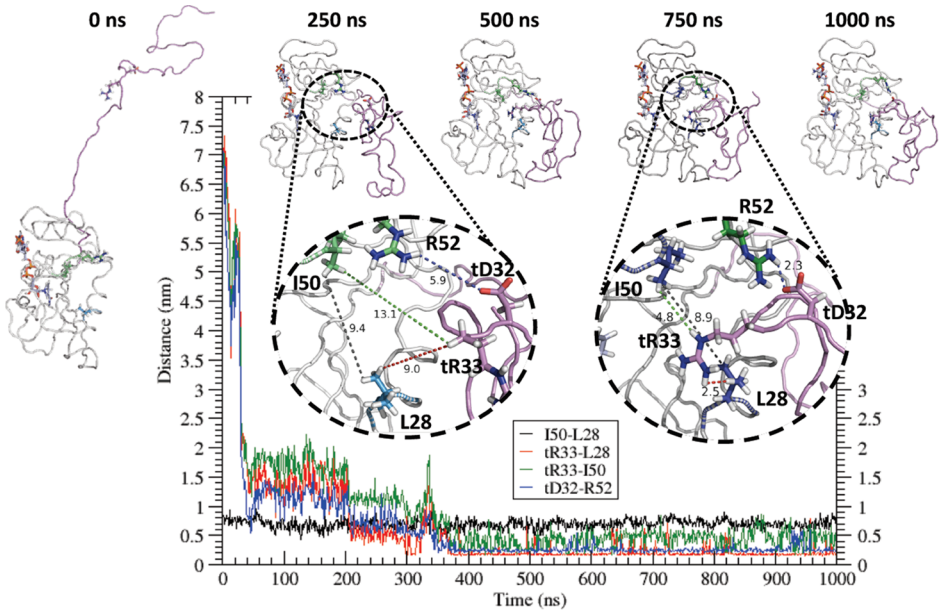

Figure 2. MD simulation on the N-terminus tag along its folding process and the minimum distances among residue pairs. The N-terminus tag folds close to the entrance of the substrate-binding cavity. Although the distance between L28 and I50 (black line) is relatively stable, the distances of residue pairs tR33-L28 (red line) and tR33-I50 (green line) decrease along with the MD simulation, indicating that the N-terminus tag could quickly fold and be close to the L28 and I50. Besides, the electrostatic interaction between tD32 (on the N-terminus tag) and the R52 drives them close to around 2 Å (blue line).

mixing in the case of most mutants. However, G121V-*ec*DHFR, M42F/G121V-*ec*DHFR, and T113V/G121V-*ec*DHFR show a relatively slow conversion process. Although M42F/G121S-*ec*DHFR and T113V/G121S-*ec*DHFR exhibit the lowest conversion level, both of them reach the endpoint rapidly, indicating that the product-binding affinity might be more substantial than the substrate-binding affinity, and such competition reaches equilibrium rapidly. In contrast, three mutants (G121V-*ec*DHFR, M42F/G121V-*ec*DHFR, and T113V/G121V-*ec*DHFR) show a slow turnover but higher conversion above 60%. Among them, M42F/G121V-*ec*DHFR is the most intriguing mutant. It fulfills conversion of 98% but reaches to endpoint after 14 min of mixing. The slower turnover indicates that this double mutation hinders the binding of ligands and the sampling time of the preorganization configuration in the catalytic center.

Molecular Dynamics Simulation. Both Met-42 and Thr-113 are not on the protein surface and interact with its nearby α helix in the van der Waals contacts. Hence, M42F and T113V should exhibit a negligible difference with wildtype in protein−surface electrostatics and minor effects on the N-terminus-tag structure. Also, Gly-121 is on the flexible βF−βG loop, and the adenosine binding subdomain and the major subdomain of *ec*DHFR are flanked by the βF−βG loop and the N-terminal. Hence, G121V and G121S should exhibit minor effects on the N-terminus-tag structure. We monitored the interaction between the N-terminus-tag and the main wildtype *ec*DHFR protein during the molecular dynamics (MD) simulation.[22−30] The root-mean-square deviation of the backbone (bbRMSD) for the 1000 ns MD run concerning the reference conformation at 0 ns and the conformation at 1000 ns (red line) are shown in Figure S1. The root-mean-square deviation of the backbone for the 1000 ns MD run indicates that the N-terminus-tag would be stable in the equilibration portion of the trajectory (>600 ns). As shown in Figure 2, the N-terminus tag folds close to the entrance of the substrate-binding cavity. Because residues L28 and I50 are at the entrance of the substrate-binding site, we monitored their distances to the residue tR33 on the N-terminus tag. Figure 2 displays the distances of residue pairs tR33-L28 (red line) and tR33-I50 (green line) with respect to simulation time, indicating that the N-terminus tag could quickly fold and be close to the L28 and I50 in 50 ns. In the equilibration portion of the simulation (600−1000 ns), the minimal distance of tR33-L28 is about 2.5 Å as well, as the tR33-I50 ranges from 3 to 7 Å, demonstrating that the N-terminus tag could fold close to the entrance of H_2F binding site. Such a configuration might prevent H_2F from binding to the *ec*DHFR. The driving force pulling the N-terminus tag to the H_2F-binding entrance might be the electrostatic interaction between tD32 on the N-terminus tag and the R52 of the *ec*DHFR. The tD32-R52 distance constantly narrowed down for the first 400 ns simulation. Then, the tD32-R52 distance was stably around 2 Å in the equilibration portion of the trajectory. Our 1000 ns MD simulation of the tag-DHFR suggests that the N-terminus tag might block the entrance of the H_2F binding site and interfere with the binding of H_2F. While comparing structures at 0 and 1000 ns, we observed that (1) the adenosine binding subdomain leans closer to αF and the entrance of cofactor binding site becomes smaller; (2) the distance between I50 and the nicotinamide-ribose moiety of NADPH becomes larger; (3) the Met20 loop moves away from the active site. These changes might also influence the binding of NADPH.

Cofactor-Binding Assays. The structure of the *ec*DHFR complex with the oxidized cofactor and substrate analogue is shown in Figure 1 with five intrinsic tryptophan residues (W22/W30/W47/W74/W133) labeled with blue spheres. When excited by 290 nm irradiation, *ec*DHFR is fluorescent and exhibits a fluorescence band of 300−460 nm with an emission peak at 340 nm. The emission spectrum of tryptophan and the absorption spectrum of NADPH are overlapped well, and five tryptophan residues are located

https://doi.org/10.1021/acsomega.1c02995
ACS Omega 2021, 6, 26065−26076

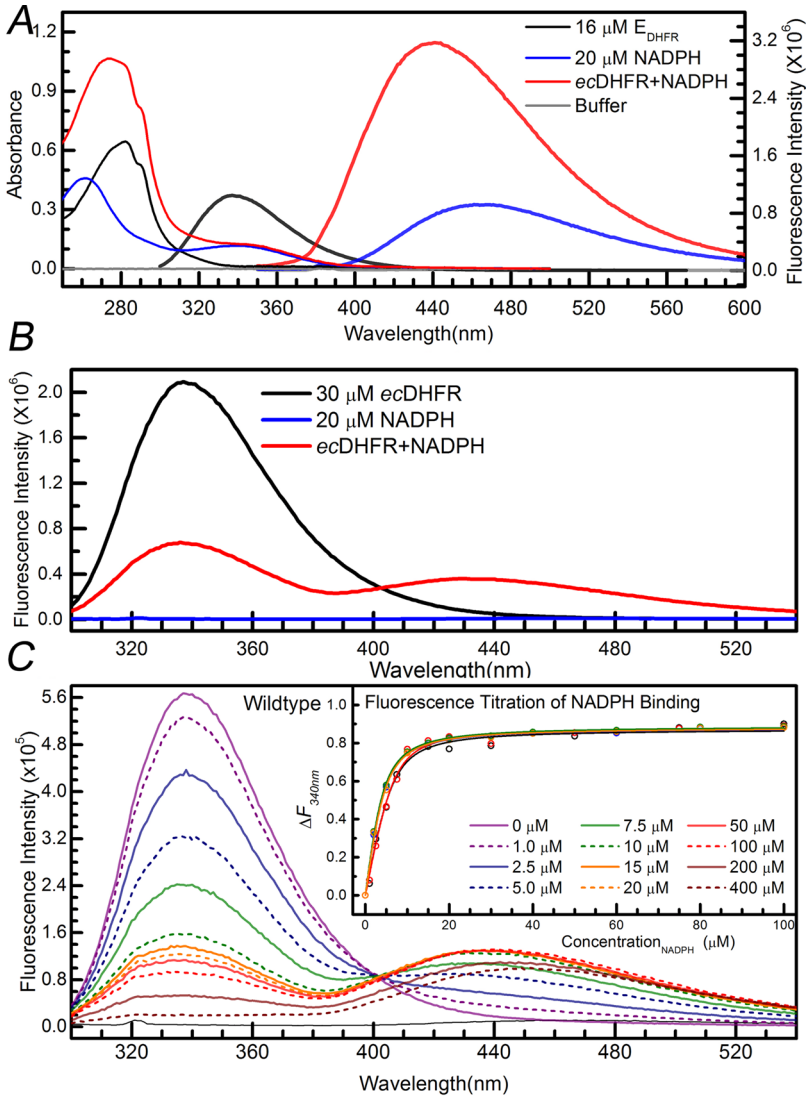

Figure 3. (A) Absorption spectra of *ec*DHFR (black line), cofactor NADPH (blue line), and the mixture (red line) of *ec*DHFR (16 μM) and cofactor NADPH (20 μM). The emission spectrum of *ec*DHFR [(black-bold line)], upon 290 nm excitation, and the emission spectrum of NADPH either in solution (blue-bold line) or the mixture (red-bold line), upon 340 nm excitation. (B) Emission spectra of *ec*DHFR (black line), cofactor NADPH (blue line), and the mixture (red line) of *ec*DHFR (30 μM) and cofactor NADPH (20 μM), under 290 nm irradiation. (C) Fluorescence spectra from the cofactor-binding titration experiments and the fluorescence spectrum of 50 μM NADPH (black-thin line). Inset shows the K_D analysis curves of five trials only up to 100 μM NADPH titration. The range of ΔF_{340nm} is from −0.1 to 1.1.

within 16 Å to NADPH.[5] Hence, *ec*DHFR and NADPH could be a Förster resonance energy transfer (FRET) pair.[6,8,9,19] Other ligands, such as H_2F, H_4F, and methotrexate (MTX), could not form a FRET pair with tryptophan, but they show a quenching effect on the tryptophan fluorescence of *ec*DHFR.[6,8,9,19]

Figure 3A shows absorption spectra of 16 μM wildtype-ecDHFR, 20 μM cofactor NADPH and a mixture of 16 μM *ec*DHFR and 20 μM NADPH, along with their emission spectra upon excitation by either 290 or 340 nm irradiation. Under 290 nm excitation, the 340 nm emission bands in *ec*DHFR originated from tryptophan fluorescence. Under 340 nm excitation, cofactor NADPH exhibits an emission band with a peak of 460 nm, but the emission peak shifts to 440 nm in the enzyme−cofactor mixture. Such spectral blueshifting indicates the binding of NADPH to *ec*DHFR resulting from slower solvation dynamics and a higher emitting state.[31] In an aqueous solution, the fluorescence of nicotinamide is partially quenched by collisions or by stacking with the adenine moiety.[32,33] Upon binding to *ec*DHFR, a nicotinamide−ribose moiety flips in the active-site pocket[5] (no collision and stacking with the adenine moiety), resulting in the increment of fluorescence intensity and blue shifting on the emission peak from 460 to 440 nm, as shown in Figure 3A. Figure 3B shows the emission spectra of 30 μM wildtype-ecDHFR, 20 μM NADPH, and a mixture of 30 μM *ec*DHFR and 20 μM NADPH upon 290 nm excitation. We observed a decrement at 340 nm fluorescence and an increment at 440 nm fluorescence in the mixture compared with *ec*DHFR alone. Because 20 μM NADPH shows extremely low fluorescence intensity upon 290 nm excitation, the 440 nm emission in the mixture must result from FRET between tryptophans and NADPH in the complex. FRET between tryptophan residues in enzymes, and cofactor NADPH (or NADH) was observed in many cases.[34−36]

We measured the 340 nm fluorescence intensity of *ec*DHFR at various enzyme concentrations from 500 nM up to 60 μM.

https://doi.org/10.1021/acsomega.1c02995
ACS Omega 2021, 6, 26065−26076

The nonlinearity between fluorescence intensity and enzyme concentration occurred at a protein concentration of 20 μM. Hence, all ligand-binding assays were performed with 5 μM *ec*DHFR. In Figure 3D, we show one of the NADPH-binding titrations. With the increasing concentration of NADPH, the decrease at 340 nm fluorescence and the increase at 440 nm fluorescence were observed. When the concentration of NADPH was more than 100 μM, we observed no increment but a decrement at 440 nm fluorescence. Hence, the high concentration data were not used for the dissociation constant K_D analysis and the data were only fitted up to 100 μM. The initial concentration of free *ec*DHFR is $[E_T]$ and that of NADPH is $[L_T]$. When reaching the equilibrium of the complex formation, the concentration of the E_{NADPH} complex is $[EL]_{eq}$. The dissociation constant K_D of the E_{NADPH} complex could be represented by

$$K_D = \frac{([E_T] - [EL]_{eq})([L_T] - [EL]_{eq})}{[EL]_{eq}} \quad (2)$$

Thus, $[EL]_{eq}$ could be solved as follows

$$[EL]_{eq} = \frac{1}{2}[([E_T] + [L_T] + K_D) - \sqrt{([E_T] + [L_T] + K_D)^2 - 4[E_T][L_T]}\,] \quad (3)$$

Due to FRET, the E_{NADPH} complex is not fluorescent at 340 but 440 nm. If the 340 nm fluorescence of the initial *ec*DHFR is F_0 and that of the *ec*DHFR and NADPH mixture is F_{EL}, the 340 nm fluorescent signal of the mixture is from the free *ec*DHFR in the mixture ($[E]_{free} = [E_T] - [EL]_{eq}$). Because the concentration and fluorescence intensity of *ec*DHFR were in the linear relation range, hence

$$\frac{F_{EL}}{F_0} = \frac{[E]_{free}}{[E_T]} = \frac{[E_T] - [EL]_{eq}}{[E_T]} \quad (4)$$

and

$$\Delta F_{340\,nm} = \frac{(F_0 - F_{EL})}{F_0} = \frac{[EL]_{eq}}{[E_T]} = \frac{1}{2[E_T]}[([E_T] + [L_T] + K_D) - \sqrt{([E_T] + [L_T] + K_D)^2 - 4[E_T][L_T]}\,] \quad (5)$$

As shown in the inset of Figure 3D, the data were plotted with ΔF_{340nm} as Y_{axis} and $[L_T]$ as X_{axis} and fit by a nonlinear least-squares fitting program with the eq 5, where F_0 is the initial fluorescence intensity in the absence of NADPH, F_{EL} is the fluorescence intensity in the presence of NADPH of $[L_T]$, E_T is the initial *ec*DHFR concentration, L_T is the initial NADPH concentration, and the dissociation constant K_D is the unknown parameter that was obtained by fitting results. The enzyme−cofactor dissociation constant K_D^{NADPH} of wildtype-*ec*DHFR to NADPH was estimated as 1.23 ± 0.06 μM by 340 nm fluorescence titration (Figure 3D inset). This value is about 3∼4-fold weaker than the previous reports of 0.34 and 0.44 μM.[6,8] Because the E_{NADPH} complex is not fluorescent at 340 nm but 440 nm, the 440 nm fluorescence intensity is proportional to the concentration of the E_{NADPH} complex, hence

$$F_{440\,nm} = F_{EL}^{440\,nm} - F_0^{440\,nm} = A[EL]_{eq} = \frac{A}{2}[([E_T] + [L_T] + K_D) - \sqrt{([E_T] + [L_T] + K_D)^2 - 4[E_T][L_T]}\,] \quad (6)$$

where A is the population fluorescence yield relative coefficient, F_0^{440nm} is the initial 440 nm fluorescence intensity in the absence of NADPH, and F_{EL}^{440nm} is the fluorescence intensity in the presence of NADPH of $[L_T]$. The dissociation constants K_D analyzed from two approaches, ΔF_{340nm} and F_{440nm} analyses, are pretty consistent. The comparison between the two methods is shown in Figure S2. The cofactor-binding assays were also performed with 500 nM *ec*DHFR and NADPH-titration concentrations of 25, 50, 100, 200, 250, 400, 500 nM, 1, 2, and 4 μM. The dissociation constant K_D^{NADPH} was estimated as 1.09 ± 0.45 μM by 340 nm fluorescence titration. Because the cofactor-binding assays in two different titration ranges (*ec*DHFR 500 nM and 5 μM) exhibit similar results, we further used 5 μM enzyme concentration for all the mutation experiments.

The NADPH titration with the fluorescence measurements and ΔF_{340nm} analyses of *ec*DHFR mutants are shown in Figure S3 and inset. Similar to the ΔF_{340nm} analysis in wildtype, the data in each mutant were only fitted up to 100 μM, and the corresponding enzyme−cofactor dissociation constants K_D^{NADPH} are listed in Table 1. However, to show the same

Table 1. Dissociation Constants for Wildtype DHFR and Mutants With Various Ligands

		K_D^{NADPH} (μM)	$K_D^{H_2F}$ (μM)
	wildtype	1.23 ± 0.06	2.84 ± 0.31
single-point mutation	M42F	33.64 ± 2.67	18.25 ± 2.47
	T113V	13.73 ± 1.82	43.93 ± 4.33
	G121S	9.73 ± 2.40	6.52 ± 3.05
	G121V	12.24 ± 1.41	69.41 ± 9.63
double-point mutation	M42F/G121S	115.61 ± 20.12	79.97 ± 8.85
	M42F/G121V	73.96 ± 9.09	44.70 ± 6.19
	T113V/G121S	77.49 ± 19.23	60.24 ± 7.21
	T113V/G121V	137.30 ± 1.94	75.77 ± 4.06

ΔF_{340nm} range (−0.1−1.1), single mutations up to 100 μM NADPH and double mutations up to 400 μM NADPH are displayed in the inset of the figure. In all single-point mutations, M42F-*ec*DHFR shows the weakest binding with NADPH, which might arise due to the proximity to the NADPH-binding site and bulky replacement of phenylalanine. The phenylalanine replacement induces the stereo-hindrance and affects the rotation and movement of helix αC, resulting in weakening the enzyme−ligand affinity. However, this result differs from the previous report,[8] in which the M42F-*ec*DHFR did not deviate from the wildtype behavior. In earlier studies on M42 with 14 amino acid replacements,[37] the results demonstrated that M42 is essential to stabilize the hydrophobic interactions with the residues surrounding this position. Considering the N-terminus-tag in our system, we found that the N-terminus tag pushes the adenosine binding subdomain closer to the helix αF and enhances the hindrance effect from M42F. Three other single-point mutants are one-order weaker in the binding of NADPH. All of them are located in the major subdomain and far from NADPH binding site and the N-

https://doi.org/10.1021/acsomega.1c02995
ACS Omega 2021, 6, 26065−26076

terminus tag. These results are similar to those reported previously, which indicated that G121S-*ec*DHFR and G121V-*ec*DHFR weakened NADPH binding to 10-fold and 40-fold, respectively.[6,8] While the mutation positions away from the N-terminus tag, the additive effects on the NADPH binding are not clearly observed.

All double-point mutations *ec*DHFR show that the dissociation constant K_D^{NADPH} increases around 2 orders of magnitude compared to wildtype-*ec*DHFR. The weaker the NADPH binding, the smaller the 440 nm fluorescence increment observed in the titration experiments. As shown in Scheme 1 and Table 2, the double mutant cycle analysis[38−40]

Scheme 1. General Scheme for a Double Mutant Cycle[a]

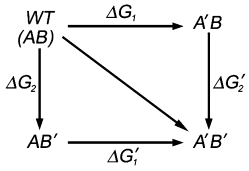

[a]Two residues A and B are mutated to A′ an B′, respectively. A′B and AB′ represent the single-point mutants and A′B′ is the corresponding double-point mutant

of double mutations demonstrates nonadditive properties upon substrate binding. In general, the first point mutation affects strongly the NADPH binding compared to the second one ($\Delta G_1 > \Delta G'_1$ and $\Delta G_2 > \Delta G'_2$).

$$\Delta G_1 = RT \ln\left(\frac{K_D^{A'B}}{K_D^{wildtype}}\right) \qquad \Delta G_2 = RT \ln\left(\frac{K_D^{AB'}}{K_D^{wildtype}}\right)$$

$$\Delta G'_1 = RT \ln\left(\frac{K_D^{A'B'}}{K_D^{AB'}}\right) \qquad \Delta G'_2 = RT \ln\left(\frac{K_D^{A'B'}}{K_D^{A'B}}\right)$$

$$\Delta G(A'B' - WT) = RT \ln\left(\frac{K_D^{A'B'}}{K_D^{wildtype}}\right)$$

$$\Delta\Delta G = \Delta G(A'B' - WT) - (\Delta G_1 - \Delta G_2)$$

Substrate-Binding Assays. Five tryptophan residues in *ec*DHFR are located within 19 Å of substrate H_2F, where W30 is at a distance of 4.8 Å to H_2F. Although H_2F could not form a FRET pair with tryptophan, a quenching effect on the tryptophan fluorescence of *ec*DHFR by H_2F was observed, as shown in Figure 4A. In Figure 4B, with the increasing concentration of H_2F, the 340 nm fluorescence decreases, and the emission peak gradually shifts from 340 to 350 nm. When carefully examining the fluorescence contribution of H_2F, H_2F exhibits weak fluorescence, as shown in Figure 4C. The fluorescence intensity increases linearly up to 20 μM of H_2F and displays a nonlinear effect at higher H_2F concentrations. We first considered the data in Figure 4C and plotted the 340 nm fluorescence of H_2F at various concentrations. Moreover, then we analyzed the raw data with polynomial fitting and simulated the fluorescence intensity curve of H_2F, as shown in Figure 4D. The autofluorescence from H_2F was removed by simple subtraction. Figure 4E shows the H_2F titration raw data, the H_2F-simulated fluorescence intensity, and the final H_2F titration-calculated data. Both the raw data and the calculated data were used to construct ΔF_{340nm} analysis. Because the nonlinear effect becomes more pronounced at high H_2F concentration, the data were only fitted up to 60 μM, as shown in the inset of Figure 4C. The enzyme−substrate dissociation constant $K_D^{H_2F}$ of wildtype-*ec*DHFR to H_2F was estimated as 2.84 ± 0.31 and 2.11 ± 0.34 μM with and without the deduction of the effect from H_2F fluorescence, respectively. When the data were only fitted up to 20 μM (analysis results not shown), the dissociation constant $K_D^{H_2F}$ of wildtype-*ec*DHFR to H_2F was estimated as 2.54 ± 0.45 μM with the deduction of the effect from H_2F fluorescence. This enzyme−substrate dissociation constant is about 9−11-fold weaker than those reported previously, 0.33 and 0.25.[6,8] From the MD simulation result, the N-terminus tag blocking the entrance of H_2F might be the main reason for the weakening H_2F binding affinity.

The H_2F titration with the fluorescence measurement and ΔF_{340nm} analysis of *ec*DHFR mutants are shown in Figure S4 and inset. Similar to the ΔF_{340nm} analysis in wildtype, the data of each mutant were only fitted up to 60 μM, and the corresponding enzyme−substrate dissociation constants $K_D^{H_2F}$ are listed in Table 1. However, to show the same ΔF_{340nm} range (−0.1−1.1), the titration analysis on single mutations up to 100 μM H_2F and on double mutations up to 200 μM H_2F was carried out. While compared to wildtype, mutants at the T113 position (T113V-*ec*DHFR, T113V/G121S-*ec*DHFR, and T113V/G121V-*ec*DHFR) weakened the H_2F binding up to a maximum of 26-fold in T113V/G121V-*ec*DHFR. Thr-113 is close to Asp-27. The hydroxyl group of T113 forms hydrogen bonding with the carbonyl group of Asp-27 and hydrogen network with cavity water (W_{405}), substrate H_2F, and Asp-27.[41] In T113V mutants, such network changes, and the H_2F binding decreases. Our results are similar to those reported previously, which indicated a 20−30 fold decrease in H_2F-binding affinity.[42]

Surprisingly, the substrate dissociation constant of G121V-*ec*DHFR is 10-fold higher than that of G121S-*ec*DHFR. Our

Table 2. Double-Mutant Cycle Analysis With NADPH and H_2F

NADPH	A′	B′	ΔG_1 (kcal/mole)	ΔG_2 (kcal/mole)	$\Delta G'_1$ (kcal/mole)	$\Delta G'_2$ (kcal/mole)	$\Delta\Delta G$ (kcal/mole)
M42F/G121S	M42F	G121S	8.20	5.12	6.13	3.06	−2.06
M42F/G121V	M42F	G121V	8.20	5.69	4.45	1.95	−3.75
T113V/G121S	T113V	G121S	5.98	5.12	5.19	4.33	−0.79
T113V/G121V	T113V	G121V	5.98	5.69	5.99	5.71	0.02
H_2F	A′	B′	ΔG_1 (kcal/mole)	ΔG_2 (kcal/mole)	$\Delta G'_1$ (kcal/mole)	$\Delta G'_2$ (kcal/mole)	$\Delta\Delta G$ (kcal/mole)
M42F/G121S	M42F	G121S	4.61	2.06	6.21	3.66	1.60
M42F/G121V	M42F	G121V	4.61	7.92	−1.09	3.22	−5.70
T113V/G121S	T113V	G121S	6.71	2.06	5.86	1.13	−0.93
T113V/G121V	T113V	G121V	6.71	7.92	0.22	1.35	−6.57

https://doi.org/10.1021/acsomega.1c02995
ACS Omega 2021, 6, 26065−26076

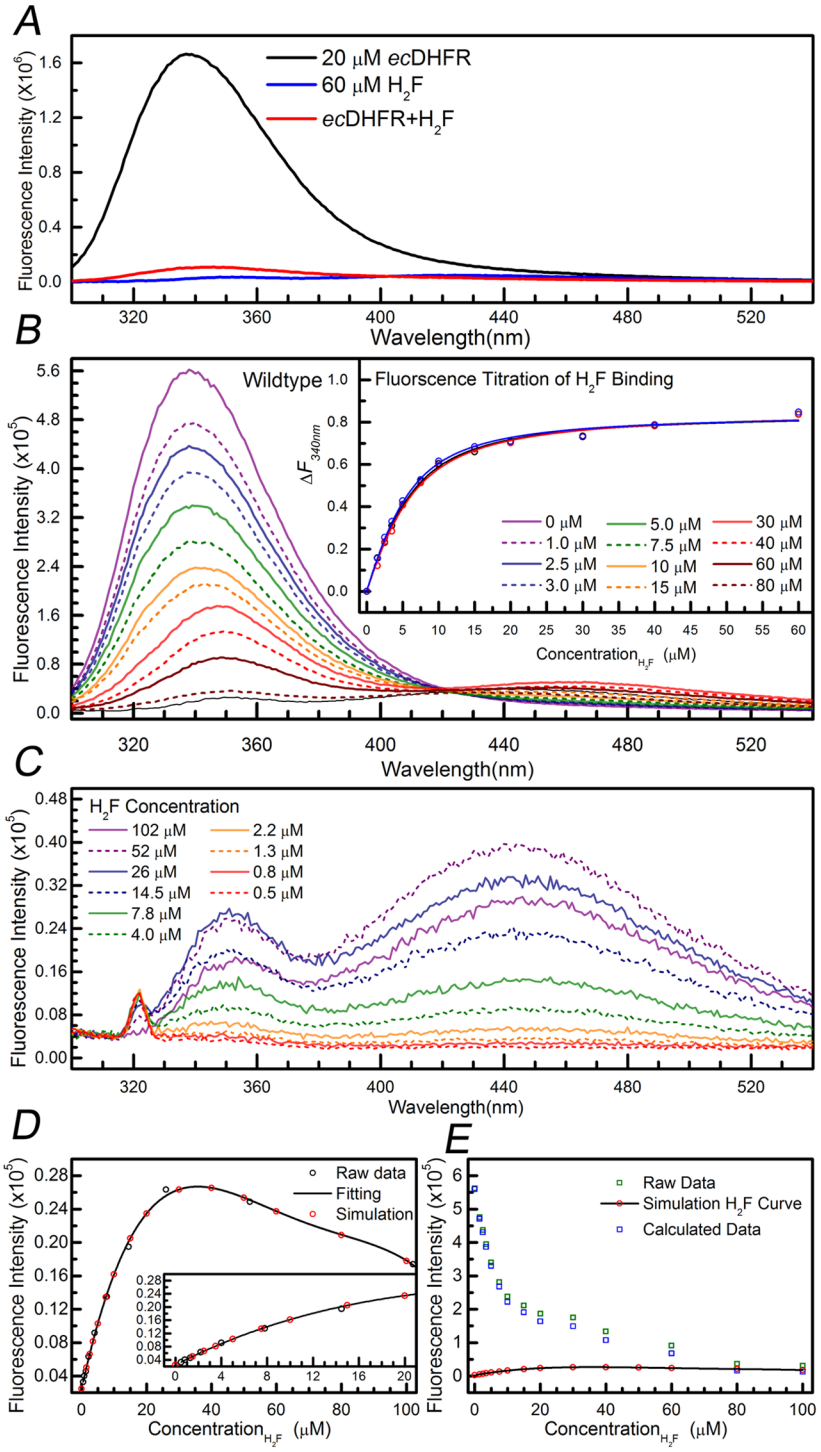

Figure 4. (A) Emission spectra of 20 μM *ec*DHFR (black line), substrate 60 μM H_2F (blue line), and the mixture (red line) of 20 μM *ec*DHFR and 60 μM substrate H_2F. In the presence of a substrate, the 340 nm tryptophan emission decreases, indicating fluorescence quenching. (B) Fluorescence spectra from the substrate-binding titration experiments and the fluorescence spectrum of 52 μM H_2F (black-thin line). The inset shows the K_D analysis curves of three trials only up to 60 μM NADPH titration based on the deduction of the H_2F effect described in (C−E). The range of ΔF_{340nm} is from −0.1 to 1.1. (C) Fluorescence spectra of H_2F at various concentrations. (D) Concentration−fluorescent intensity dependence of H_2F (black-hollow circle) was analyzed with polynomial fitting (black curve) labeled with the simulation data (red-solid circle). (E) H_2F titration raw data (green square), the H_2F-simulated fluorescence intensity (red-solid circle), and the final H_2F titration-calculated data. (blue square).

results differ from those reported previously,[8] which stated that G121S-*ec*DHFR and G121V-*ec*DHFR behaved similarly with wildtype in the H_2F-binding. Asp-122 forms hydrogen bonds with Glu-17 and Gly-15 and affect the Met20 loop conformation. In the previous studies, the correlation motion between Asp-122/Gly121 and Gly15/Glu17 is observed in wildtype. Such correlation motion becomes unclear in the G121S mutant and is even hardly observed in the G121V

https://doi.org/10.1021/acsomega.1c02995
ACS Omega 2021, 6, 26065−26076

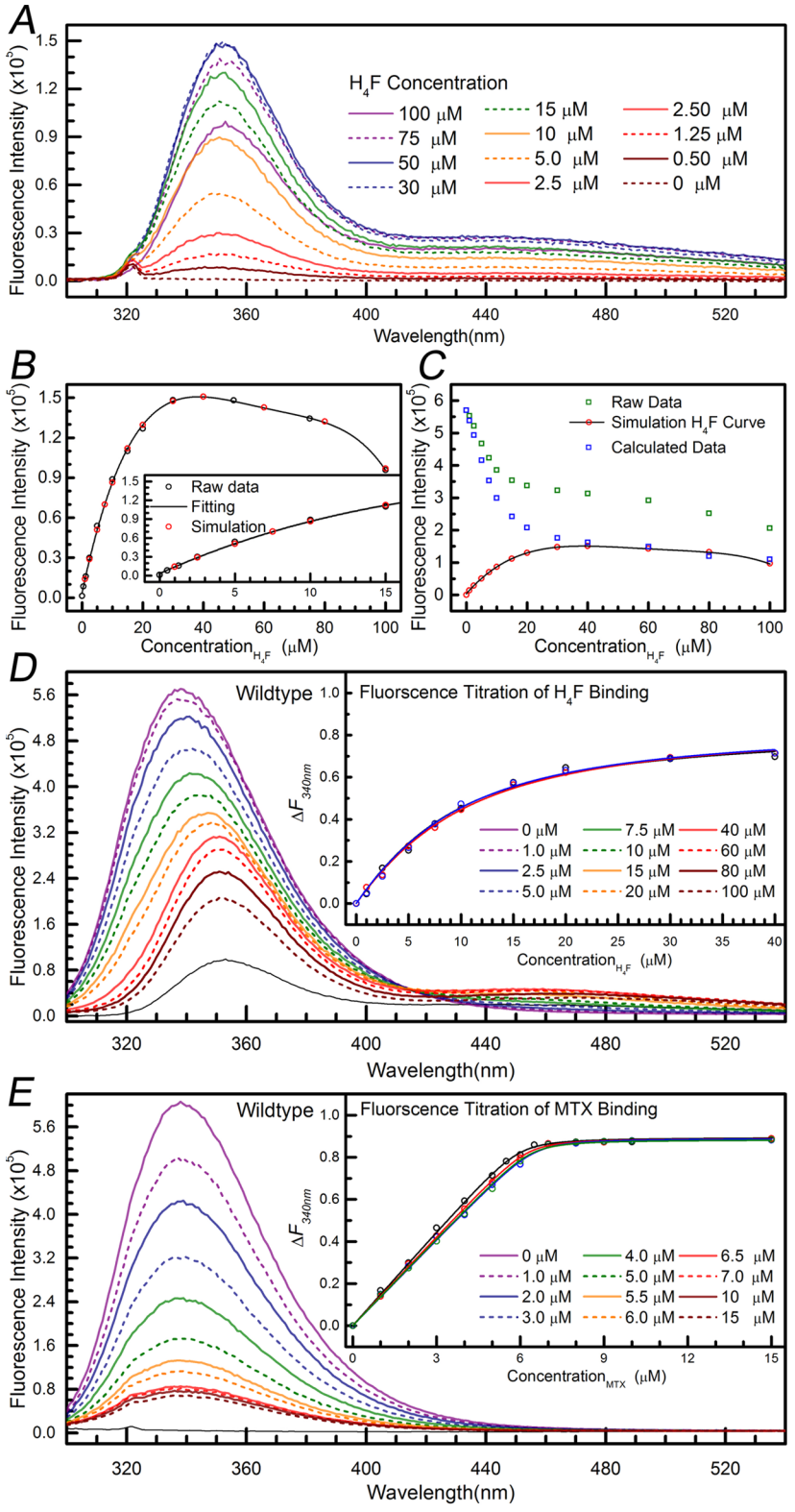

Figure 5. (A) Fluorescence spectra of H_4F at various concentrations. (B) Concentration-fluorescent intensity dependence of H_4F (black-hollow circle) was analyzed with polynomial fitting (black curve) labeled with the simulation data (red-solid circle). (C) H_4F titration raw data (green square), the H_4F-simulated fluorescence intensity (red-solid circle), and the final H_4F titration-calculated data (blue square). (D) Fluorescence spectra from the product-binding titration experiments and the fluorescence spectrum of 100 μM H_4F (black-thin line). With the increasing concentration of H_4F, the decrease at 340 nm fluorescence was observed. The inset shows the K_D analysis curves of two trials based on the deduction of the H_4F effect describe in (A–C). (E) Fluorescence spectra from the inhibitor-binding titration experiments and the fluorescence spectrum of 15 μM MTX (black-thin line). The inset shows the K_D analysis curves of four trials.

https://doi.org/10.1021/acsomega.1c02995
ACS Omega 2021, 6, 26065−26076

mutant.[9] The Gly-121 mutations might exhibit a similar effect on protein flexibility, as reported for Asp-122 mutations.[41] This G121V-mutation effect might be less critical in the flexible enzyme and results in similar dissociation constants in G121S-*ec*DHFR and G121V-*ec*DHFR, as shown in previous studies.[6,8,9] However, in our enzymes, the N-terminus tag acts as a cap on the entrance of the substrate-binding site. Hence, the G121V-mutation effect reinforces the compact H_2F-binding site, leading to much weaker binding to the substrate. Also, based on MD simulation, the N-terminus tag causes the Met20 loop to move away from the active site. The Val residues is a bulky and nonpolar sidechain, and it weakens the interaction between Asp-122 and the Met20 loop and possibly affects the H_2F-binding site. However, in G121S-*ec*DHFR, the hydroxyl group of Ser residue might participate in the hydrogen network, resulting in a minor effect on the interaction between Asp-122 and the Met20 loop and the H_2F binding.

As shown in Table 2, the double mutant cycle analysis[38−40] of double mutations demonstrates nonadditive properties upon substrate binding. The effect of G121V and T113V mutation overwhelms that of G121S and M42F. Hence, in M42F/G121V-*ec*DHFR and T113V/G121V-*ec*DHFR, we observed that $\Delta G_1 \gg\gg \Delta G'_1$. In T113V/G121S-*ec*DHFR and T113V/G121V-*ec*DHFR, we observed that $\Delta G_2 \gg\gg \Delta G'_2$.

Product-Binding and Inhibitor-Binding Assays. The effects of ligand autofluorescence and inner filter effect are more enhanced with the H_4F ligand, as shown in Figure 5A. The original H_4F titration raw data, the polynomial fitting, the H_4F-simulated fluorescence intensity, and the final H_4F titration-calculated data are shown in Figure 5B,C. One of the H_4F titration experiments is shown in Figure 5D. The 340 nm fluorescence decreases, and the emission peak significantly shifts from 340 to 350 nm. Both the raw data and the calculated data were used to construct ΔF_{340nm} analysis. Because the nonlinear effect becomes more pronounced at high concentration, the data were fitted only up to 40 μM. The enzyme−product dissociation constant $K_D^{H_4F}$ of wildtype-*ec*DHFR to H_4F was estimated as 6.05 ± 0.41 and 4.57 ± 0.47 μM with and without the deduction of the effect from H_4F fluorescence, respectively. The compact substrate/product binding site resulting from the N-terminus tag weakens the product binding about 40-fold compared with the previous results.[6,8] The inhibitor MTX exhibits no fluorescence, and one of the MTX titration experiments is shown in Figure 5E. The 340 nm fluorescence decreases dramatically, and the enzyme−inhibitor dissociation constant K_D^{MTX} in wildtype-*ec*DHFR was estimated as 42.6 ± 2.6 nM. Interestingly, this value is about 8-fold stronger than that reported previously, which is 362 nM in solution.[19] Also, this value is 4-fold weaker than that reported by the studies of 9.5 nM on single-molecule studies.[18] The inhibitor MTX and substrate H_2F are similar in dimension but are different in the functional group. We assumed that the N-terminal tag affects the k_{on} association rate of these two ligands similarly. However, upon binding, the influence of the N-terminal tag on the k_{off} dissociation rate of these two ligands should be significantly different. In addition, the effects from the N-terminus tag might change upon binding to coverglass. As shown in Figure S5, the enzyme−product dissociation constants $K_D^{H_4F}$ of M42F-*ec*DHFR and T113V-*ec*DHFR were estimated as 44.01 ± 2.73 and 40.87 ± 2.23 μM, respectively. These two mutants show similar enzyme−product dissociation constants but with the H_2F-to-H_4F conversion of 98 and 74% (Figure 1), respectively. When the enzymatic reaction progressed, the concentration of H_2F decreased, and the concentration of H_4F increased. There is an affinity competition between substrate and product. In M42F-*ec*DHFR ($K_D^{H_4F} = 2.6 \times K_D^{H_2F}$) and T113V-*ec*DHFR ($K_D^{H_4F} = 1.0 \times K_D^{H_2F}$), competition on the binding of product and substrate contributes to the final conversion percentage. In M42F-*ec*DHFR, the enzyme binds to the substrate more tightly than the product, leading to higher productivity. In contrast, in T113V-*ec*DHFR, the enzyme binds to the substrate and the product with a similar tendency, leading to lower productivity.

CONCLUSIONS

Based on enzyme activity assays, we confirmed that all enzymes could convert H_2F to H_4F and measured the extent of reaction under nonsaturation conditions thermodynamically. When the enzymatic reaction progressed, the concentration of H_2F decreased, and the concentration of H_4F increased. There is an affinity competition between the substrate and product in the presence of the cofactor. The dissociation constants $K_D^{H_2F}$ and $K_D^{H_4F}$ in wildtype *ec*DHFR are 2.84 and 6.05 μM, respectively. While $[H_2F] \approx 15$ μM and $[H_4F] \approx 35$ μM, ligands and 5 μM wildtype *ec*DHFR formed the same amount of the E_{H_2F} complex and E_{H_4F} complex in solution. However, the reaction reached about 96%, which indicated the affinity competition between the substrate and product is different in the presence of a cofactor. In the presence of the cofactor, the dissociation constant $K_D^{H_4F}$ would become much larger than $K_D^{H_2F}$. In the previous studies, the dissociation constant of H_4F increases about 110 times in the presence of the cofactor ($\frac{K_{D\ between\ E^{NADPH}\ and\ H_2F}}{K_{D}\ between\ ecDHFR\ and\ H_2F} = 110$).[6]

We selected residues at highly conserved positions Met-42, Thr-113, and Gly-121 and designed several mutations, including single-point and double-point mutations. The optical approaches with the FRET effect and fluorescence quenching upon ligand binding were demonstrated. We systematically measured the equilibrium thermodynamic dissociation constant for enzyme−cofactor, enzyme−substrate, and enzyme−product complex in wildtype *ec*DHFR and each mutant. In the M42F-*ec*DHFR mutant, we propose that the stereo-hindrance phenylalanine residue squeezes and affects the rotation and movement of helix αC, resulting in the weakening enzyme−ligand affinity. In the T113V-*ec*DHFR mutant, because the valine and threonine residues are similar in size, this mutation does not create significant space disturbance. However, valine lacks the hydroxyl group as threonine and affects the hydrogen network in the H_2F binding, leading to decreasing H_2F binding. Mutations at the Gly-121 position might affect the protein flexibility dependent on the type of replacement. In G12lV-*ec*DHFR mutation, such an effect leads to much weaker binding to the substrate. In the double-mutant-cycle analysis, double mutations show nonadditive properties upon either cofactor or substrate binding. Also, in general, the first point mutation strongly affects the ligand binding ($\Delta G_1 > \Delta G'_1$ and $\Delta G_2 > \Delta G'_2$) compared to the second one.

As shown in Figure 2, the N-terminus tag is an additional peptide at the N-terminus. It acts as a cap on the substrate entrance, pushes the adenosine binding subdomain to the helix αF, and influences the binding of NADPH in most mutants. If the mutation positions are away from the N-terminus tag and the adenosine binding subdomain, the additive effects due to

https://doi.org/10.1021/acsomega.1c02995
ACS Omega 2021, 6, 26065−26076

the N-terminus tag were not observed. The bioseq-*ec*DHFR protein studied here provides insights into the impact of the N-terminus tag. Using a biotin-tag enzyme in fluorescence correlation spectroscopy studies is the main reason to have *ec*DHFR attached with the N-terminus tag. This biotinylated tag will be used to attach *ec*DHFR to the coverglass surface through avidin. The effects from the N-terminus tag might change upon binding to coverglass. As discussed previously, K_D^{MTX} (42.6 ± 2.6 nM) measured here is between the none-N-terminus tag studies in solution (362 nM)[19] and the N-terminus tag studies on coverglass (9.5 nM).[18]

MATERIALS AND METHODS

Plasmid Design and Protein Expression and Purification. The *E. coli* DHRF sequence (*ec*DHFR Uniprot: P0ABQ4) with the N-terminal insert containing a 19-residue lysine biotinylation signal sequence (MGLNDIFEAQKIEWHGGGT; bioseq)[18] was subcloned into the *BamHI* and *EcoRI* sites of pRSETa plasmid. The designed pRESTa-bioseq-*ec*DHFR plasmid was constructed through DNA synthesis services by Genscript with DNA sequence confirmation. Due to the low expression level, the bioseq-*ec*DHFR DNA sequence was further subcloned into the *BamHI* and *EcoRI* sites of the pET28a plasmid. The pET28a-bioseq-*ec*DHFR construct was used to express *ecDHFR* as the previous report with some modifications.[18] Briefly, *E. coli* BL21(DE3)-pLysS cells containing the plasmid pET28a-bioseq-*ec*DHFR were grown at 37 °C in LB broth containing 50 mg/L kanamycin to the absorption of 0.6 at 600 nm and induced at 37 °C for 5−8 h with 0.3 mM isopropyl-β-D-1-thiogalactopyranoside. After harvesting, the 6Histag-bioseq-*ec*DHFR protein was purified by an ÄKTA prime plus liquid chromatography system with HisTrap HP columns (Ni Sepharose affinity resin) followed by a Hiprep-26/60 desalting column. With a gradient elution from 10 to 500 mM imidazole in 50 mM PBS buffer containing 500 mM NaCl at pH 8.0, the bioseq-*ec*DHFR protein was eluted between 150 and 255 mM imidazole. After desalting and dialysis, the 6Histag-bioseq-*ec*DHFR protein was stored at MTEN buffer consisting of 50 mM 2-(N-morpholino) ethane sulfonate (MES), 25 mM Tris, 100 mM NaCl, 0.1 mM EDTA, and 25 mM ethanolamine at 7.4 pH.[20] All enzyme assays and ligand-binding assays were carried out within 3 days of storage in 4 °C.

Three highly conserved positions, Met-42 (M42), Thr-113 (T113), and Gly-121(G121), were selected. Site-directed mutagenesis steps were carried out with QuikChange Lightning Site-directed Mutagenesis kit (StrateGene) to engineer the following mutations: (1) single-point mutation: M42F-*ec*DHFR, T113V-*ec*DHFR, G121S-*ec*DHFR, and G121V-*ec*DHFR; (2) double-point mutation: M42F/G121S-*ec*DHFR, M42F/G121V-*ec*DHFR, T113V/G121S-*ec*DHFR, and T113V/G121V-*ec*DHFR. The *ec*DHFR mutants with a double-point mutation formed inclusion bodies, while they were induced at 37 °C. Therefore, all cell cultures were quickly cooled down and induced at 20 °C for 18−24 h with 0.3 mM isopropyl-β-D-1-thiogalactopyranoside.

Enzyme Activity Assays. The activity of *ec*DHFR was determined at 25 °C following the decrease of NADPH and 7,8-dihydrofolate (H_2F) by the absorbance measurements at 340 nm using the Hitachi double beam spectrophotometer (U-3900) in MTEN buffer as described above. *ec*DHFR and NADPH were mixed to form an E_{NADPH}−complex sample. The E_{NADPH}−complex sample and H_2F were then mixed to form a reaction solution with starting concentrations of 5 μM *ec*DHFR, 100 μM NADPH, and 50 μM H_2F for carrying out the enzyme assays. The reaction solutions were kept at 25 °C, while the absorption measurements were performed for 15 min. Enzyme assays for wildtype and each mutant were carried out at least three times. Because *ec*DHFR and $NADP^+$ exhibit no absorption at 340 nm, the initial point and the final point of the reaction were estimated with a mixture of 100 μM NADPH and 50 μM H_2F and a mixture of 50 μM NADPH and 50 μM 5,6,7,8-tetrahydrofolate (H_4F), respectively. The concentrations of compounds in solution were determined by UV absorbance using the following molar extinction coefficient: NADPH (ε_{340} = 6.22 mM^{-1} cm^{-1}), $NADP^+$(ε_{260} = 18 mM^{-1} cm^{-1}), H_2F (ε_{282} = 28 mM^{-1} cm^{-1}), H_4F (ε_{297} = 28 mM^{-1} cm^{-1}), and MTX (ε_{302} = 22.1 mM^{-1} cm^{-1}).[21] All the reagent concentrations refer to the final concentrations in the reaction mixture unless otherwise specified. Ligands, such as NADPH (Sigma N5130), H_2F (Sigma D7006), H_4F (Sigma T3125), and MTX (Sigma M9929), were purchased from Sigma-Aldrich and used directly without further purification. The stationary absorption and fluorescence spectra were recorded with a spectrophotometer (U-3900, Hitachi High-Tech.) and a fluorimeter (FluoroMax4, HORIBA Jobin Yvon Inc).

Molecular Dynamics Simulation. Because there are additional histag and 19-residue lysine biotinylation signal sequences at the N-terminus of *ec*DHFR, to understand the effect of the extra N-terminus-tag on the ligand-binding affinity, we tracked the N-terminus tag folding process. We monitored the interaction between the N-terminus tag and the main *ec*DHFR protein. The starting structure of the *ec*DHFR was from PDB (PDB ID: 1RX1).[5] In this structure, the reduced form NADPH binds to *ec*DHFR. The N-terminus tag was generated by protein structure prediction server (PS) version 3.0.[22] Simulation parameters of the NADPH were generated using the program ACPYPE with Antechamber.[23,24] All simulations were performed with the GROMACS[25] version 2018, and the AMBER99SB force field was used in this study. The *ec*DHFR and N-terminus tag *ec*DHFR structures were in boxes, respectively, filled with 7096 and 35,616 TIP3P water molecules, and the buffer distance of 1.0 nm was used in molecular dynamics simulation. Sodium ions were added to both systems to neutralize the system charge, and PropKa was used to set the protonated state of all residues at pH 7.4. The long-range electrostatic interactions were computed by the smooth particle-mesh Ewald (PME) algorithm, while short-range electrostatic and van der Waals cutoffs were set to 1.4 nm.[26,27]

For each system, after carrying out the relaxation of the system by the steepest descent minimization, 200 ps simulation with protein restraints was conducted to equilibrate the solvent and ion positions around the proteins at constant temperature 300 K. Random initial velocities according to the Maxwell distribution at 300 K were generated for each run. The temperatures of 298 and 300 K displayed a negligible difference in the Maxwell distribution and no effect on the structure of *ec*DHFR. Both *ec*DHFR and N-terminus tag *ec*DHFR systems were then simulated for 1000 ns using a time step of 2 fs, while constraining all bond lengths with the P-LINCS algorithm.[28] The temperature was kept at 300 K using the V-rescale thermostat,[29] and the pressure was maintained at 1 bar using the Parrinello−Rahman barostat.[30]

Ligand-Binding Assays. The *ec*DHFR contains five intrinsic tryptophan residues (W22/W30/W47/W74/W133).

https://doi.org/10.1021/acsomega.1c02995
ACS Omega 2021, 6, 26065−26076

When excited by 290 nm irradiation, *ec*DHFR is fluorescent and exhibits a fluorescence band of 300−460 nm with an emission peak at 340 nm. The emission spectrum of tryptophan and the absorption spectrum of NADPH are overlapped well, and five tryptophan residues are located within 16 Å to NADPH.[5] Hence, *ec*DHFR and NADPH could be a Förster resonance energy transfer (FRET) pair. Other ligands, such as H_2F, H_4F, and methotrexate (MTX), could not form a FRET pair with tryptophan, but they show a quenching effect on the tryptophan fluorescence of *ec*DHFR. The 340 nm fluorescence intensity of *ec*DHFR at different enzyme concentrations was measured to perform all experiments in the linear relation range. The equilibrium thermodynamic dissociation constant (K_D) was determined by titration with the increasing ligand concentration. We prepared an *ec*DHFR of 5 μM with various concentrations of the ligand range of 500 nM to 400 μM. The fluorescence spectra in each mixing sample were measured from 300 to 570 nm under the 290 nm irradiation. Each data set included at least three independent experiments, and each experiment is an average of at least two measurements under the same conditions.

■ ASSOCIATED CONTENT

Supporting Information

The Supporting Information is available free of charge at https://pubs.acs.org/doi/10.1021/acsomega.1c02995.

Root-mean-square deviation of the backbone, comparison between $\Delta F_{340\ nm}$ and $F_{440\ nm}$ analyses in wildtype DHFR, cofactor-binding titration experiments on (A∼D) single-point mutation and (E∼H) double-point mutation, substrate-binding titration experiments on (A∼D) single-point mutation and (E∼H) double-point mutation, and K_D analysis curves of M42F and T113V (PDF)

■ AUTHOR INFORMATION

Corresponding Author

Ya-Ting Kao − *Department of Biological Science and Technology, Institute of Bioinformatics and Systems Biology, and Center For Intelligent Drug Systems and Smart Bio-devices (IDS2B), National Yang Ming Chiao Tung University, Hsinchu 30068 Taiwan, ROC*; orcid.org/0000-0002-9245-6560; Email: yatingkao@nycu.edu.tw

Authors

Chen-Hua Huang − *Institute of Bioinformatics and Systems Biology, National Yang Ming Chiao Tung University, Hsinchu 30068 Taiwan, ROC*

Yun-Wen Chen − *Institute of Bioinformatics and Systems Biology, National Yang Ming Chiao Tung University, Hsinchu 30068 Taiwan, ROC*

Tsun-Tsao Huang − *Institute of Bioinformatics and Systems Biology, National Yang Ming Chiao Tung University, Hsinchu 30068 Taiwan, ROC*

Complete contact information is available at: https://pubs.acs.org/10.1021/acsomega.1c02995

Author Contributions

‖C.-H.H. and Y.-W.C. contributed equally to this work.

Notes

The authors declare no competing financial interest.

Accession ID for *E. coli* Dihydrofolate reductase: folA: P0ABQ4 (https://www.uniprot.org/uniprot/P0ABQ4).

■ ACKNOWLEDGMENTS

This work was supported by grants from the Ministry of Science and Technology, Taiwan (MOST 101-2113-M-009-024-MY2, MOST 103-2113-M-009-012-MY2, and MOST 108-2113-M-009-022-) and the Center for Intelligent Drug Systems and Smart Bio-devices (IDS^2 B) in Taiwan.

■ REFERENCES

(1) Schweitzer, B. I.; Dicker, A. P.; Bertino, J. R. Dihydrofolate reductase as a therapeutic target. *FASEB J.* **1990**, *4*, 2441−2452.

(2) Raimondi, M.; Randazzo, O.; La Franca, M.; Barone, G.; Vignoni, E.; Rossi, D.; Collina, S. DHFR inhibitors: reading the past for discovering novel anticancer agents. *Molecules* **2019**, *24*, 1140.

(3) Matthews, D.; Alden, R.; Bolin, J.; Freer, S.; Hamlin, R.; Xuong, N.; Kraut, J.; Poe, M.; Williams, M.; Hoogsteen, K. Dihydrofolate reductase: x-ray structure of the binary complex with methotrexate. *Science* **1977**, *197*, 452−455.

(4) Bystroff, C.; Kraut, J. Crystal structure of unliganded Escherichia coli dihydrofolate reductase. Ligand-induced conformational changes and cooperativity in binding. *Biochemistry* **1991**, *30*, 2227−2239.

(5) Sawaya, M. R.; Kraut, J. Loop and subdomain movements in the mechanism of Escherichia coli dihydrofolate reductase: crystallographic evidence. *Biochemistry* **1997**, *36*, 586−603.

(6) Cameron, C. E.; Benkovic, S. J. Evidence for a functional role of the dynamics of glycine-121 of Escherichia coli dihydrofolate reductase obtained from kinetic analysis of a site-directed mutant. *Biochemistry* **1997**, *36*, 15792−15800.

(7) Agarwal, P. K.; Billeter, S. R.; Rajagopalan, P. T. R.; Benkovic, S. J.; Hammes-Schiffer, S. Network of coupled promoting motions in enzyme catalysis. *Proc. Natl. Acad. Sci. U.S.A.* **2002**, *99*, 2794−2799.

(8) Rajagopalan, P. T. R.; Lutz, S.; Benkovic, S. J. Coupling interactions of distal residues enhance dihydrofolate reductase catalysis: mutational effects on hydride transfer rates. *Biochemistry* **2002**, *41*, 12618−12628.

(9) Rod, T. H.; Radkiewicz, J. L.; Brooks, C. L., III Correlated motion and effect of distal mutations in dihydrofolate reductase. *Proc. Natl. Acad. Sci. U.S.A.* **2003**, *100*, 6980−6985.

(10) Wong, K. F.; Selzer, T.; Benkovic, S. J.; Hammes-Schiffer, S. Impact of distal mutations on the network of coupled motions correlated to hydride transfer in dihydrofolate reductase. *Proc. Natl. Acad. Sci. U.S.A.* **2005**, *102*, 6807−6812.

(11) Mauldin, R. V.; Lee, A. L. Nuclear magnetic resonance study of the role of M42 in the solution dynamics of Escherichia coli dihydrofolate reductase. *Biochemistry* **2010**, *49*, 1606−1615.

(12) Boehr, D. D.; Schnell, J. R.; McElheny, D.; Bae, S.-H.; Duggan, B. M.; Benkovic, S. J.; Dyson, H. J.; Wright, P. E. A distal mutation perturbs dynamics amino acid networks in dihydrofolate reductase. *Biochemistry* **2013**, *52*, 4605−4619.

(13) Singh, P.; Sen, A.; Francis, K.; Kohen, A. Extension and limits of the network of coupled motions correlated to hydride transfer in dihydrofolate reductase. *J. Am. Chem. Soc.* **2014**, *136*, 2575−2582.

(14) Villafranca, J. E.; Howell, E. E.; Voet, D. H.; Strobel, M. S.; Ogden, R. C.; Abelson, J. N.; Kraut, J. Direct mutagenesis of dihydrofolate reductase. *Science* **1983**, *222*, 782−788.

(15) Howell, E. E.; Villafranca, J. E.; Warren, M. S.; Oatley, S. J.; Kraut, J. Functional role of aspartic acid-27 in dihydrofolate reductase revealed by mutagenesis. *Science* **1986**, *231*, 1123−1128.

(16) Appleman, J. R.; Howell, E. E.; Kraut, J.; Blakley, R. L. Role of aspartate 27 of dihydrofolate reductase from Escherichia coli in interconversion of active and inactive enzyme conformers and binding of NADPH. *J. Biol. Chem.* **1990**, *265*, 5579−5584.

(17) Liu, C. T.; Francis, K.; Layfield, J. P.; Huang, X.; Hammes-Schiffer, S.; Kohen, A.; Benkovic, S. J. Escherichia coli dihydrofolate reductase catalyzed proton and hydride transfers: temporal order and

the roles of Asp27 and Tyr100. *Proc. Natl. Acad. Sci. U.S.A.* **2014**, *111*, 18231−18236.
(18) Rajagopalan, P. T. R.; Zhang, Z.; McCourt, L.; Dwyer, M.; Benkovic, S. J.; Hammes, G. G. Interaction of dihydrofolate reductase with methotrexate: ensemble and single-molecule kinetics. *Proc. Natl. Acad. Sci. U.S.A.* **2002**, *99*, 13481−13486.
(19) Fierke, C. A.; Benkovic, S. J. Probing the functional role of threonine-113 of Escherichia coli dihydrofolate reductase for its effect on turnover efficiency, catalysis, and binding. *Biochemistry* **1989**, *28*, 478−486.
(20) Williams, J. W.; Morrison, J. F.; Duggleby, R. G. Methotrexate, a high-affinity pseudosubstrate of dihydrofolate reductase. *Biochemistry* **1979**, *18*, 2567−2573.
(21) Miller, G. P.; Benkovic, S. J. Deletion of a highly motional residue affects formation of Michaelis complex for Escherichia coli dihydrofolate reductase. *Biochemistry* **1998**, *37*, 6327−6335.
(22) Huang, T. T.; Hwang, J. K.; Chen, C. H.; Chu, C. S.; Lee, C. W.; Chen, C. C. $(PS)^2$: protein structure prediction server version 3.0. *Nucleic Acids Res.* **2015**, *43*, W338−W342.
(23) Sousa da Silva, A. W.; Vranken, W. F. ACPYPE-AnteChamber PYthon Parser interfacE. *BMC Res. Notes* **2012**, *5*, 367.
(24) Wang, J.; Wang, W.; Kollman, P. A.; Case, D. A. Automatic atom type and bond type perception in molecular mechanical calculations. *J. Mol. Graph. Model.* **2006**, *25*, 247−260.
(25) Abraham, M. J.; Murtola, T.; Schulz, R.; Páll, S.; Smith, J. C.; Hess, B.; Lindahl, E. GROMACS: high performance molecular simulations through multi-level parallelism from laptops to supercomputers. *SoftwareX* **2015**, *1*−*2*, 19−25.
(26) Darden, T.; York, D.; Pedersen, L. Particle mesh Ewald : an N·Log(N) method for Ewald sums in large systems. *J. Chem. Phys.* **1993**, *98*, 10089−10092.
(27) Essmann, U.; Perera, L.; Berkowitz, M. L.; Darden, T.; Lee, H.; Pedersen, L. G. A smooth particle mesh Ewald method. *J. Chem. Phys.* **1995**, *103*, 8577−8593.
(28) Hess, B. P-LINCS: A parallel linear constraint solver for molecular simulation. *J. Chem. Theory Comput.* **2008**, *4*, 116−122.
(29) Bussi, G.; Donadio, D.; Parrinello, M. Canonical sampling through velocity rescaling. *J. Chem. Phys.* **2007**, *126*, 014101.
(30) Parrinello, M.; Rahman, A. Polymorphic transitions in single crystals: a new molecular dynamics method. *J. Appl. Phys.* **1981**, *52*, 7182−7190.
(31) Zhang, L.; Kao, Y.-T.; Qiu, W.; Wang, L.; Zhong, D. Femtosecond studies of tryptophan fluorescence dynamics in proteins: local solvation and electronic quenching. *J. Phys. Chem. B* **2006**, *110*, 18097−18103.
(32) Dunn, S. M. J.; King, R. W. Kinetics of ternary complex formation between dihydrofolate reductase, coenzyme, and inhibitors. *Biochemistry* **1980**, *19*, 766−773.
(33) Gafni, A.; Brand, L. Fluorescence decay studies of reduced nicotinamide adenine dinucleotide in solution and bound to liver alcohol dehydrogenase. *Biochemistry* **1976**, *15*, 3165−3171.
(34) Townley, H. E.; Sessions, R. B.; Clarke, A. R.; Dafforn, T. R.; Griffiths, W. T. Protochlorophyllide oxidoreductase: A homology model examined by site-directed mutagenesis. *Protein* **2001**, *44*, 329−335.
(35) Fjeld, C. C.; Birdsong, W. T.; Goodman, R. H. Differential binding of NAD^+ and NADH allows the transcriptional corepressor carboxyl-terminal binding protein to serve as a metabolic sensor. *Proc. Natl. Acad. Sci. U.S.A.* **2003**, *100*, 9202−9207.
(36) Chen, S.; Fahmi, N. E.; Bhattacharya, C.; Wang, L.; Jin, Y.; Benkovic, S. J.; Hecht, S. M. Fluorescent biphenyl derivatives of phenylalanine suitable for protein modification. *Biochemistry* **2013**, *52*, 8580−8589.
(37) Ohmae, E.; Fukumizu, Y.; Iwakura, M.; Gekko, K. Effects of mutation at methionine-42 of Escherichia coli dihydrofolate reductase on stability and function: implication of hydrophobic interactions. *J. Biochem.* **2005**, *137*, 643−652.
(38) Carter, P. J.; Winter, G.; Wilkinson, A. J.; Fersht, A. R. The use of double mutants to detect structural changes in the active site of the tyrosyl-tRNA synthetase (Bacillus stearothermophilus). *Cell* **1984**, *38*, 835−840.
(39) Fersht, A. R.; Wells, T. N. C. Linear free energy relationships in enzyme binding interactions studied by protein engineering. *Protein Eng.* **1991**, *4*, 229−231.
(40) Pagano, L.; Toto, A.; Malagrinò, F.; Visconti, L.; Jemth, P.; Gianni, S. Double mutant cycles as a tool to address folding, binding, and allostery. *Int. J. Mol. Sci.* **2021**, *22*, 828.
(41) Mhashal, A. R.; Pshetitsky, Y.; Eitan, R.; Cheatum, C. M.; Kohen, A.; Major, D. T. Effect of Asp122 mutation on the hydride transfer in E. coli DHFR demonstrates the goldilocks of enzyme flexibility. *J. Phys. Chem. B* **2018**, *122*, 8006−8017.
(42) Chen, J.-T.; Mayer, R. J.; Fierke, C. A.; Benkovic, S. J. Site-specific mutagenesis of dihydrofolate reductase from Escherichia coli. *J. Cell. Biochem.* **1985**, *29*, 73−82.

https://doi.org/10.1021/acsomega.1c02995
ACS Omega 2021, 6, 26065−26076